Performance Index for in Home Assessment of Motion Abilities in Ataxia Telangiectasia: A Pilot Study

M. El Arayshi [1], **C. M. Verrelli** [1,*], **G. Saggio** [1], **M. Iosa** [2,3], **A. E. Gentile** [4], **L. Chessa** [5], **M. Ruggieri** [6] **and A. Polizzi** [7]

[1] Electronic Engineering Department, University of Rome Tor Vergata, 00133 Rome, Italy; elarayshi@ing.uniroma2.it (M.E.A.); saggio@uniroma2.it (G.S.)

[2] Department of Psychology, Sapienza University of Rome, 00185 Rome, Italy; marco.iosa@uniroma1.it

[3] IRCCS Santa Lucia Foundation, 00179 Rome, Italy

[4] National Centre for Rare Diseases, Istituto Superiore di Sanità, 00162 Rome, Italy; amaliaegle.gentile@iss.it

[5] Department of Clinical and Molecular Medicine, Sapienza University Foundation, 00185 Rome, Italy; luciana.chessa@fondazione.uniroma1.it

[6] Unit of Rare Diseases of the Nervous System in Childhood, Department of Clinical and Experimental Medicine, University of Catania, 95131 Catania, Italy; martino.ruggieri@unict.it

[7] Department of Educational Science, University of Catania, 95131 Catania, Italy; agata.polizzi1@unict.it

* Correspondence: verrelli@ing.uniroma2.it; Tel.: +39-(0)-6-72597410

Abstract: *Background.* It has been shown in the very recent literature that human walking generates rhythmic motor patterns with hidden time harmonic structures that are represented (at the subject's comfortable speed) by the occurrence of the golden ratio as the the ratio of the durations of specific walking gait subphases. Such harmonic proportions may be affected—partially or even totally destroyed—by several neurological and/or systemic disorders, thus drastically reducing the smooth, graceful, and melodic flow of movements and altering gait self-similarities. *Aim.* In this paper we aim at, preliminarily, showing the reliability of a technologically assisted methodology—performed with an easy to use wearable motion capture system—for the evaluation of motion abilities in Ataxia-Telangiectasia (AT), a rare infantile onset neurodegenerative disorder, whose typical neurological manifestations include progressive gait unbalance and the disturbance of motor coordination. *Methods.* Such an experimental methodology relies, for the first time, on the most recent accurate and objective outcome measures of gait recursivity and harmonicity and symmetry and double support subphase consistency, applied to three AT patients with different ranges of AT severity. *Results.* The quantification of the level of the distortions of harmonic temporal proportions is shown to include the qualitative evaluations of the three AT patients provided by clinicians. *Conclusions.* Easy to use wearable motion capture systems might be used to evaluate AT motion abilities through recursivity and harmonicity and symmetry (quantitative) outcome measures.

Keywords: gait analysis; wearable sensors; rhythmic motor pattern; time harmonic structure; golden ratio; neurological disorders

1. Introduction

Ataxia Telangiectasia (**AT**; MIM # 208900) is a rare genetic disorder characterized by early onset ataxia (lack of coordination of movements), neurodegeneration and multisystem involvement, including immunological defects, organ failure and predisposition to cancer [1,2]. The incidence worldwide is estimated to span from 1:40,000 to 1:100,000 individuals, and 1:300,000 in the West Midlands population. From a clinical point of view, AT is characterized by impaired coordination of the movement of voluntary muscles, with gait unbalance, oculomotor apraxia, altered speech fluency, anterior horn cell degeneration, peripheral neuropathy, and a cerebellar cognitive affective psychological profile. Despite the disease affecting, overall, the central and peripheral nervous system, the involvement

of other organs and body systems is variably present. Cutaneous and ocular telangiectasia, growth failure, dysfunction of the immune system with immune deficiency, recurrent respiratory infections, endocrine and gastrointestinal disturbances, proneness to malignancy, premature aging, and hypersensitivity to ionizing radiations, are part of the clinical constellation. The phenotypic spectrum of the disease varies from the severe classical form, presenting with the early onset, relentless progression of neurodegeneration and reduced survival, to the mild variant form, where the clinical picture is consistent with the later onset of the disease, slow progression of ataxia, and longer survival.

Apart from cerebellar ataxia, which is the most common neurological manifestation of AT that gives the syndrome its name, AT encompasses a wide spectrum of movement disorders that complicates patients' daily activities while impacting the course of the disease [1,3]. At the onset, initial manifestations of AT include cerebellar features with gait unbalance, hypotonia, and slow voluntary movements followed by dystonia, choreoathetosis, and tremor, while the occurrence of movement disorders at follow up confirms, in almost all patients, the progression of cerebellar manifestations with standing and posture troubles, myoclonus, dystonia, choreoathetosis, and tremor. The age of onset of ataxia is generally coincident with the beginning of children walking, at around 12–13 months, however, signs of head tilting and mild truncal ataxia may be apparent at earlier developmental ages. Age of diagnosis is generally postponed to 3–4 years, pointing out a diagnostic delay of about 2 years (personal observation) for this syndrome. The ongoing loss of coordination and balance, together with the degeneration of anterior horn cells, and peripheral neuropathy lead to a loss of ambulation usually occurring in classic AT between the ages of 12 and 16 years, with some patients becoming wheelchair bound earlier. Joint contractures develop insidiously due to the progressive lack of motor activity and diminished weight gain. Walking capacities can range from normal to abnormal with an irregular, staggering, and wide based gait. Patients can be unable to walk with their feet in a tandem position (the heel to toe position of both feet), walk without support, or walk at all, and be wheelchair bound. Gait speed can also be affected, varying from normal, slightly, or strikingly reduced. Standing capacity is impaired by a significant sway and continuous posture corrections of the body [3].

Management of AT is entrusted to tailored support and lifelong rehabilitative programs. Difficulties in accessing specialized clinical care prompt the need for advanced and cutting edge techniques, which are, thus, deservedly thought of as essential sources to ameliorate the quality of life of AT patients and their families. However, thanks to the growing body of knowledge, traditional rehabilitative approaches are now more often flanked by fascinating experimental investigations, leading to the more independent management of the disease from the patient's point of view, while also allowing more frequent and long-lasting patient training. In general, body movement can be monitored using several different technologies, with the optoelectronic ones being considered as the gold standard, which are mainly based on infrared cameras. However, because of drawbacks such as high costs, dedicated rooms, and the necessity of experienced personnel, other technologies have been emerging. Therefore, depending on the particular body movement to be measured, different solutions have been proposed: photoplethysmogram (PPG), ballistocardiogram (BCG), seismocardiogram (SCG) for measuring respiratory rate [4]; WiFi and radio detection and ranging (RADAR) for activity recognition [5]; and wearable technology—based on inertial measurement units (IMUs) [6], flexible sensors [7], insole pressure sensors, or electromyography sensors—for gait analysis [8,9].

Within the frame of clinical or general performance evaluations [10–15], temporal gait analyses are nowadays used to complement the classical gait analyses that involve motion analysis, dynamic electromyography, force plate recordings, energy cost measurements, and measurement of the stride characteristics [16–18]. Indeed, four time intervals—namely, the ones associated with the durations of the gait cycle, swing, stance, and double support phases—temporally characterize symmetric and recursive human walking [16]. An innovative research direction, promoted by [19], has emerged from most of the literature

agreeing that the foot off reliably occurs at 60% to 62% of a physiological gait when the subject is (symmetrically and recursively) walking at a comfortable speed: the analysis of the ratio between the swing and double support phase durations has experimentally recognized it as close—in healthy subjects symmetrically and recursively walking at about 4 km/h [20], but not in patients affected by neurological disorders—to the golden ratio $\phi = (1 + \sqrt{5})/2 \approx 1.618$, i.e., the positive solution to the equation $x^2 = 1 + x$ (see [21]). Such an irrational number, which is related to Euclid's problem of cutting in a self-proportional way a given straight segment, thus captures:

- Self-similarity features in symmetric walking of healthy subjects; and
- A reduction of the smooth, graceful and melodic flow of movement in the altered gait of patients (e.g., patients with Parkinson's Disease, known to be characterized by a tremor at rest, rigidity, akinesia or bradykinesia, and postural instability [22]; patients with cerebellar ataxia [13] (for patients with cerebellar ataxia and healthy subjects, energy consumption during walking is shown to be minimized when they walk with a gait ratio close to the golden ratio [13]), or patients with stroke [23]).

Now, symmetry and harmony are strictly intertwined in walking. Two comprehensive indices in ref. [24,25] have been, accordingly, recently suggested to simultaneously characterize these two important features. In particular, ref. [25] has provided original mathematically founded arguments to a fractal approach to the question (the generic idea that walking can have a fractal structure can be found in [26], while the existence of significant alterations from such a structure in patients with Parkinson's Disease has been suggested in [27]): the larger scale structure resembles the subunit structure through the generation of a self-referential loop (see Refs. [28,29] for relevant applications to swimming). Human walking is, then, innovatively described in terms of generalized finite length Fibonacci sequences [30] and dynamics on graph concepts, with the new mathematical concept of a *composite gait cycle*—involving two specific couples of overlapping gait cycles, namely, the left and right gait cycles and the *adjoint* right and left gait cycles—to extend the idea of stride to stride intervals [31] and step-by-step intervals [32].

The aim of this paper is to present the reliability of a technologically assisted methodology—performed with an easy to use wearable motion capture system—in assessing motion abilities in AT. Such a methodology relies on the experimental verification of the most recent and comprehensive accurate and objective outcome measures of gait recursivity and harmonicity and symmetry and double support sub phase consistency, as very recently defined in [25]. Three subjects with different ranges of severity of AT are analyzed and the values of the involved indices are shown to comply with the qualitative evaluations provided by the clinicians.

2. Materials and Methods

In this section, the outcome measures of gait recursivity and harmonicity and symmetry and double support subphase consistency (defined in [25]) are first recalled. The technologically assisted methodology, performed with the easy to use wearable Movit motion capture system, is then described, along with the experimental set up and data acquisition modality. The features of the participants, including the three subjects with different ranges of severity of AT, are, finally, reported.

2.1. Fibonacci Sequence Based Index

Consider the walking gait [19,33] and let: GC stand for gait cycle; FS stand for foot strike; FO stand for foot off; r and l stand for right and left, respectively; adj stand for adjoint; ST stand for stance; SW stand for swing; and DS stand for double support. The reader is referred to the comprehensive modelling of Figure 1, which reports the right and left gait cycles, with durations GC_r, GC_l, as the time intervals (or phases) between two consecutive strikes of the right foot ($FS_{r,a}$, $FS_{r,b}$), and two consecutive lift off of the left foot ($FO_{l,a}$, $FO_{l,b}$), respectively, such that the same right swing phase appearing in the left stance phase is the one that is involved in the definition of the right gait cycle. Analogously, the *adjoint* right

and left gait cycles, with durations $\mathrm{GC}_r^{\mathrm{adj}}$, $\mathrm{GC}_l^{\mathrm{adj}}$, are the time intervals (or phases) between two consecutive lift offs of the right foot ($\mathrm{FO}_{r,x}$, $\mathrm{FO}_{r,y}$) and two consecutive strikes of the left foot ($\mathrm{FS}_{l,x}$, $\mathrm{FS}_{l,y}$), respectively, with $\mathrm{FO}_{r,x}$ and $\mathrm{FS}_{l,x}$ immediately preceding $\mathrm{FS}_{r,a}$ and $\mathrm{FO}_{r,x}$, respectively. As clarified in [25], each stance includes both the double support subphase with the left foot behind and the right foot ahead and the double support subphase with the right foot behind and left foot ahead. Accordingly, the double support consistency consists of the equal partition of the double support sub-phases, i.e., $\mathrm{DS}_x = \mathrm{DS}_y$ (and $\mathrm{DS}_w = \mathrm{DS}_y$, $\mathrm{DS}_y = \mathrm{DS}_z$). With respect to this, it is worth recalling that gait symmetry and recursivity often decay in pathological walking.
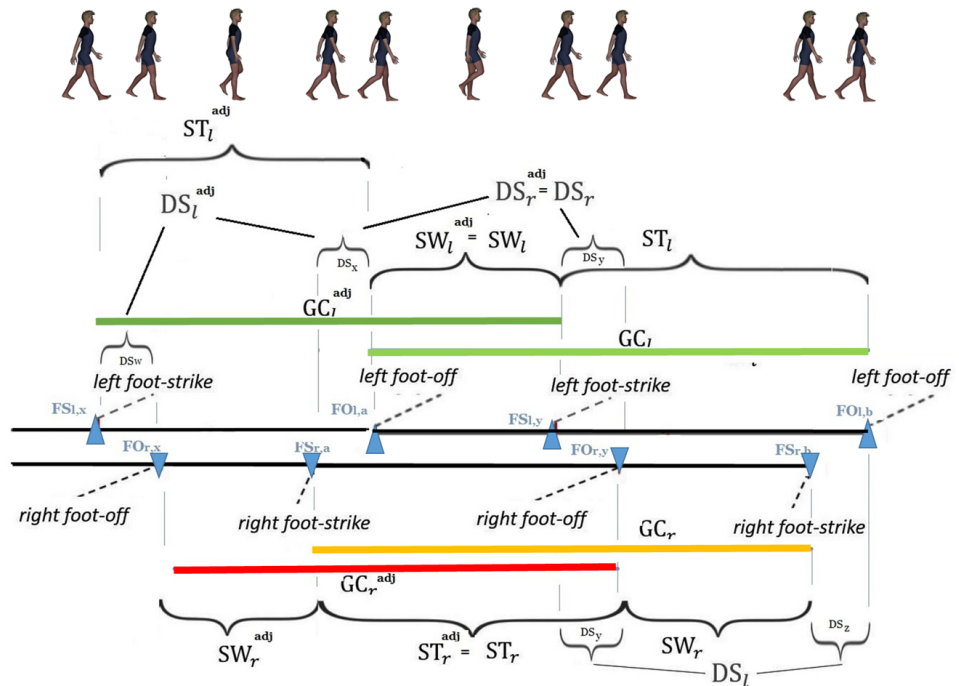
Figure 1. *Composite gait cycle*: right and left gait cycles and *adjoint* right and left gait cycles.

Let the right (respectively, left) stance have time duration ST_r (respectively, ST_l). The durations of the right swing and left swing phases [19] are given by:

$$\mathrm{SW}_r = \mathrm{GC}_r - \mathrm{ST}_r, \quad \mathrm{SW}_l = \mathrm{GC}_l - \mathrm{ST}_l. \tag{1}$$

Furthermore, the duration DS_r (respectively, DS_l) of the right (respectively, left) double support phase is given by:

$$\mathrm{DS}_r = \mathrm{ST}_r - \mathrm{SW}_l \quad (\mathrm{DS}_l = \mathrm{ST}_l - \mathrm{SW}_r). \tag{2}$$

The durations DS_r and DS_l, in turn, satisfy $\mathrm{DS}_r = \mathrm{DS}_x + \mathrm{DS}_y$, $\mathrm{DS}_l = \mathrm{DS}_y + \mathrm{DS}_z$. On the other hand, the same quantities (durations) are introduced in [25] for the *adjoint* right and left gait cycles. They are denoted by $\mathrm{ST}_r^{\mathrm{adj}}$, $\mathrm{ST}_l^{\mathrm{adj}}$, $\mathrm{SW}_r^{\mathrm{adj}}$, $\mathrm{SW}_l^{\mathrm{adj}}$, $\mathrm{DS}_r^{\mathrm{adj}}$, $\mathrm{DS}_l^{\mathrm{adj}}$ and satisfy, by definition (see Figure 1): $\mathrm{DS}_r^{\mathrm{adj}} = \mathrm{DS}_r$, $\mathrm{SW}_l^{\mathrm{adj}} = \mathrm{SW}_l$, $\mathrm{ST}_r^{\mathrm{adj}} = \mathrm{ST}_r$. Again, the durations $\mathrm{DS}_r^{\mathrm{adj}}$ and $\mathrm{DS}_l^{\mathrm{adj}}$, in turn, satisfy $\mathrm{DS}_r^{\mathrm{adj}} = \mathrm{DS}_x + \mathrm{DS}_y$ and $\mathrm{DS}_l^{\mathrm{adj}} = \mathrm{DS}_w + \mathrm{DS}_x$.

Now define the quantities $\Delta\mathrm{SW} = \mathrm{SW}_l - \mathrm{SW}_r$, $\Delta\mathrm{SW}^{\mathrm{adj}} = \mathrm{SW}_l^{\mathrm{adj}} - \mathrm{SW}_r^{\mathrm{adj}}$. The following proposition recognizes the existence of special Fibonacci sequences in walking.

Proposition 1. *Let* $c_I = ST_r$, $c_{II} = ST_l$, $d_I = GC_r + \Delta SW$, $d_{II} = GC_l - \Delta SW$. *The two sequences*

$$
\begin{array}{llll}
I & : & a_I, & b_I, & c_I, & d_I \\
II & : & a_{II}, & b_{II}, & c_{II}, & d_{II}
\end{array}
\tag{3}
$$

are (generalized) 4-length Fibonacci sequences, with generators: $a_I = DS_r$, $b_I = SW_l$, and $a_{II} = DS_l$, $b_{II} = SW_r$, respectively. The same holds for the corresponding adjoint sequences (notice that the two sequences, I and I^{adj}, coincide, owing to: $DS_r^{adj} = DS_r$, $SW_l^{adj} = SW_l$, $ST_r^{adj} = ST_r$)*

$$
\begin{array}{llll}
I^{adj} & : & a_I^{adj}, & b_I^{adj}, & c_I^{adj}, & d_I^{adj} \\
II^{adj} & : & a_{II}^{adj}, & b_{II}^{adj}, & c_{II}^{adj}, & d_{II}^{adj}
\end{array}
\tag{4}
$$

relying on: $a_I^{adj} = DS_r^{adj}$, $b_I^{adj} = SW_l^{adj}$, $a_{II}^{adj} = DS_l^{adj}$, $b_{II}^{adj} = SW_r^{adj}$, $c_I^{adj} = ST_r^{adj}$, $c_{II}^{adj} = ST_l^{adj}$, $d_I^{adj} = GC_r^{adj} + \Delta SW^{adj}$ and $d_{II}^{adj} = GC_l^{adj} - \Delta SW^{adj}$. The golden ratio ϕ thus is a fixed point for the ratios b_I/a_I, c_I/b_I, d_I/c_I and b_{II}/a_{II}, c_{II}/b_{II}, d_{II}/c_{II}, with the same again happening for the adjoint sequences.*

Now, let λ, δ, μ^{adj}, λ^{adj} be positive weights. Given positive reals ξ_n, ξ_d, ξ_v, define the normalized quantity:

$$
\left(\frac{\xi_n}{\xi_d} - \xi_v \right)^2_n = \left(\frac{\xi_n}{\xi_d} \right)^{-1} \left(\frac{\xi_n}{\xi_d} - \xi_v \right)^2.
\tag{5}
$$

The Φ-*bonacci gait number* (which is the most natural generalization to a nonsymmetric and recursive walking case, and of the corresponding gait ratio $|SW/DS - \phi|$, defined in [19,22] for symmetric walking; while it simply incorporates a weighted modification of the index $= |\Delta SW|/\overline{SW}$ in [34], evaluated at both the gait and the adjoint gait) is defined in [25] (no conjecture based quantity is here introduced) as

$$
\mathcal{Y}_\Phi = \sqrt{ \left(\frac{SW_l}{DS_r} - \phi \right)^2_n + \left(\frac{SW_r}{DS_l} - \phi \right)^2_n + \mu^{adj} \left(\frac{SW_r^{adj}}{DS_l^{adj}} - \phi \right)^2_n }
$$
$$
+ \lambda \sqrt{ \left(\frac{SW_r}{SW_l} - 1 \right)^2_n + \lambda^{adj} \left(\frac{SW_r^{adj}}{SW_r} - 1 \right)^2_n } + \delta \sqrt{ \left(\frac{DS_x}{DS_y} - 1 \right)^2_n }.
\tag{6}
$$

and aims at representing the recursive self-similarity and swing symmetry contributions to the gait, in conjunction with the *double support consistency*. A zero value for those indices thus describes the case in which recursivity, self-similarity, swing symmetry, and *double support consistency* occur, while the gains characterizing the previous expression can be freely chosen by the user for specific analysis requirements.

2.2. Movit System

Movit System G1 by Captiks is a wearable wireless system for motion capture and motion analysis. The system is composed of wearable small inertial devices (Movit) (Figure 2) and a receiver (Dongle). Each Movit communicates wirelessly with the Dongle, which is connected to the PC via a USB port. The Movit system exploits a proprietary communication protocol (2.4 GHz, based on IEEE 802.15.4 MAC) that allows synchronization and sending of data from multiple sensors (from 1 up to 16 devices) at a high sample rate (200 Hz in internal storage mode and up to 100 Hz in real time mode).

Figure 2. Movit devices.

Each Movit (dimension W 48 mm × H 39 mm × D 18 mm, weight 40 gr) hosts different sensors, in particular, a 3-axis accelerometer and a 3-axis gyroscope (±2 g to ±16 g and ±250 dps to ±2000 dps, respectively, by MPU 9250 by InvenSense, San Jose, CA, USA). A 40 MHz clocked microcontroller (AT32UC3A4256 by Atmel, San Jose, CA, USA) handles data that can be internally stored and/or transmitted wirelessly. A Li-Po battery supplies the Movit G1 with up to six hours of operational mode. Each Movit, in addition to the raw data of the accelerometer and gyroscope, provides its orientation in the space through a 6 DoF quaternion. Thanks to a patented two-step calibration, the orientation of each sensor can be mapped to the orientation of the body joints, to allow the reconstruction of kinematics and anatomical angles. The first calibration step consists of acquiring 3 positions obtained with 2 rotation movements of 90 deg (using the calibration base) for the definition of a unique reference coordinate system. The second calibration step consists of the acquisition of the T pose (standing position with arms parallel to the ground) to align the Movit System to the body coordinate system. The application of sensors on the patient's body is easy and immediate. The elastic bands are applied directly to the patient's clothes and are equipped with a coating that limits their movement. The sensors are positioned on the bands using plastic support (Dock) equipped with Velcro to make everything applicable on any physical conformation. The Movit System G1 was originally validated through a video based gold standard system [35] (Vicon, by Oxford Metrics). The testing was realized by measuring different subjects performing different motor exercises (walking and joint movements) and the results demonstrated excellent accuracy and repeatability. In particular, the RMSE errors for the joint angles in the sagittal plane are <3.5 deg, the Pearson correlation coefficients for hip, knee, and ankle in the sagittal plane are >0.97 and the percentage errors of spatio-temporal parameters in the gait test are <5%. The system is supplied with: (i) Motion Studio for recording session and system set up; (ii) Motion Analyzer for analyzing session and obtaining a pdf report related to the specific test. The Motion Studio allows for recording the movement from many points of view. The synchronization between raw data (accelerometer, gyroscope), joint angles, 3D animation, and video allows a study at different levels, making the analysis even more complete. It also gives the possibility to set up the transmission frequencies, the accelerometers, and gyroscope full scale range (from ±2 g to ±16 g and from ±250 dps to ±2000 dps, respectively), the recording mode (memory or real time mode) and the system calibration. Advantageously (especially in the considered application requiring the computation of temporal gait quantities), it is not mandatory to establish an exact measurement site for the Movit device, so they can be located anywhere but within the same body district. The most significant criterion for sensor position is the symmetricity between the left and right half of the body (i.e., the sensors positioned on the right arm and forearm should be on the same line as sensors on the left arm and forearm, and the same for sensors on the lower half of the body). This is in agreement with similar findings obtained in [36].

2.3. Data Acquisition and Signal Processing

Walking tests of 9 meters long (4.5-meters-long for F.) in an open area are performed by the three AT patients, while 8-meter-long walking tests in a hallway are performed by healthy subjects. A network of 13 wearable lightweight sensors of the Movit System G1 is used. The sensors are located on the principal body parts (head, Arm, forearm, chest, hip, thigh, leg and foot). Further details are reported hereafter.

- Head: the sensor is centered on the upper half of the head front (parallel to the coronal plane);
- Arm: the sensor is located near the biceps brachii, oriented to the back (parallel to the coronal plane) [arm sensor position is relative to the body standing in the T position, with palm in parallel with the transverse plane];
- Forearm: the sensor is located on the lower forearm, oriented to the top (parallel to the transverse plane) [forearm sensor position is relative to the body standing in the T position, with palm in parallel with the transverse plane];
- Chest: the sensor is centered between the shoulder blades on the back (parallel to the coronal plane);
- Hip: the sensor is located on the back of the hip line (parallel to the coronal plane);
- Thigh: the sensor is located on the upper thigh, oriented to the outside (parallel to the median plane);
- Leg: the sensor is located under the calf thig,h oriented to the outside (parallel to the median plane); and
- Foot: the sensor is located at the middle of the back of the foot (parallel to the transverse plane).

The temporal analysis concerns one portion of gaits in the middle of the straight path. The sequence of time instants corresponding to the right heel strike, left toe off, left heel strike, and right toe off fortwo subsequent gaits is derived using an ad hoc extraction algorithm processing the acquisitions provided by the aforementioned sensor system (see Figure 3 for details). Data from three different measurement sessions are collected for each healthy subject (and then the mean values for each quantity involved in the computation of the indices are derived) and from one single measurement session for the pathological subjects.
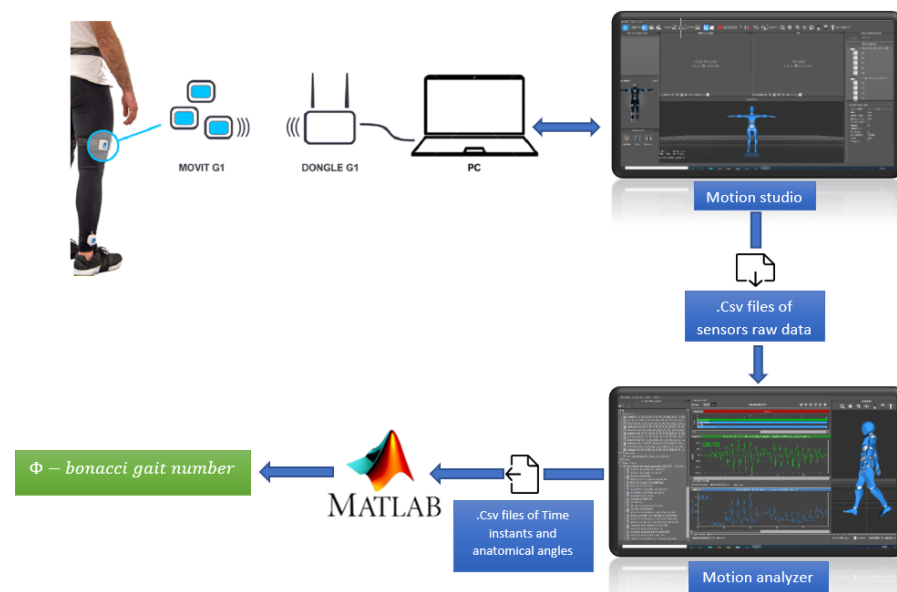
Figure 3. Flow chart. The wearable wireless sensors start to acquire and record the movement data in their internal memory with a sample rate of 200 Hz after the recording button is pressed on the user

interface of the Motion Studio software. The movement data (.csv file) for each sensor are downloaded using the Motion Studio software by connecting all the sensors to the PC via the USB cable. The data file contains: device name, bone name, timestamp, 3-axis accelerometer data in unit "g", 3-axis gyroscope data in unit "dps", accelerometer/gyroscope range, and sample rate. The sensor data file is loaded in the Motion Analyzer software for data fusion and processing to generate the time instants of the heel strike and toe off for the left and right feet, in addition to the anatomical angles. The aforementioned information coming from data processing is loaded in a dedicated MATLAB algorithm that recognizes the time instants for the gait cycle and the adjoint gait cycle subphases, involved in the computation of the Φ-bonacci gait number.

2.4. Participants

Experimental data concern three AT patients with different ranges of severity of AT—they are described hereafter (the age of the patients is intended to be at the moment of experiment)—and three healthy subjects (male, 27 years old, 1.77 m, 75.4 kg; female, 22 years old, 1.66 m, 75 kg; male, 23 years old, 1.71 m, 76 kg), all of them walking at their comfortable speed (1.32, 0.2, 1.15, 1.13, 1.167, 1.2 m/s, respectively (the neurologically severe impairments of patient F are the cause of of the low walking speed)). The healthy subjects, who play the role of a (non-age matched) control group, are here used to assess the low magnitude of their Φ-bonacci gait number, in light of the results of [25]. In particular, healthy subjects are selected as male/female controls in the age range 20–30 years and without any neurological or orthopedic deficits as representative of the physiology and biomechanics of mature walking. The features of the AT patients are reported hereafter.

- A is a 29-year-old woman who developed, by the age of 3 years, all the classic manifestations of AT; increased alpha-fetoprotein levels were initially detected. The diagnosis was confirmed by molecular analysis of the *ATM* gene and the absence of ATM protein expression. Contrary to what was expected in the classic form of AT, by the age of 12 years, ataxia slowly disappeared, and a mild choreic movement disturbance has been the only neurologic finding since then. Now, she is an independent person who has obtained a satisfying job and practices sports. Her quality of life is said to be rather good by herself. A diagnosis of the mild form of AT was made at follow up.

- F is a 35-year-old man who began to show motor developmental troubles from 9 months of life, at which age he was hypotonic and lost the ability to keep a sitting position whereas wide based ambulation was evident at 23 months. Concurrently, intentional tremors, incoordination, and stance unsteadiness manifest. A diagnosis of AT was carried out when he was 3-years-old, on the grounds of his clinical examination, serum IgA deficiency, elevated alpha-fetoprotein, and atrophic cerebellar vermis. Molecular confirmation of *ATM* gene mutations was obtained a few years later. Since the age of 11 yrs, F has been able to stand and walk only with support, language has been dysarthric, and there have occurred truncal and gait ataxia, dystonic posture of neck and hands, marked choreo-athethotic movements, and absent knees reflexes. The course of the disease was steadily progressive. At the present age of 37 yrs, he is neurologically severely impaired, can walk less than 10 m only with strong support, and is unable to sit for more than 10 min without continuous support. He pronounces only single words understandably. Since childhood, he has undergone respiratory physiotherapy at most twice a week, and, overall, for not more than 45 min per session. However, due to family job problems and the distance of his home from the hospital services, rehabilitative treatment has been, since the beginning, very discontinuous. F has been diagnosed as being a long-term survivor patient with classic AT.

- G is a 7-year-old boy, the second born of apparently healthy parents. Early psychomotor milestones were normal until the age of 15 months, when a wide-based gait, unsteadiness, and dystonic posture of hands were noticed. At that time, a brain MRI was normal. However, due to the clinical picture, the elevated alpha-fetoprotein level, and the occurrence of the compound heterozygosity of the *ATM* gene, a final diagnosis of AT was given. When examined at 2 yrs of age, clear truncal and gait ataxia, together

with hand dystonia, were observed. Over the following 5 years, ataxia moderately worsened, and generalized hypotonia, muscle weakness with fine motor deficits and uncoordinated movements, marked drooling and brisk knee reflexes developed. Since the onset of gait and motor dysfunction, the child has been put on a program of psychomotricity and respiratory therapy for two days/week, he also practices horse therapy and swimming every other day.

3. Results

All the data for the AT patients are summarized in Tables 1–3, while the ones for the healthy subjects are reported in Tables 4–6. Each of these tables report, in order: (i) the elements of sequence *I* in (3); (ii) the elements of sequence *II* in (3); (iii) the consecutive ratios between the elements of sequence *I*; (iv) the consecutive ratios between the elements of sequence *II*; and (v) the same elements and ratios for the adjoint quantities in (4). In particular, they include (the reader is referred to Figure 1): $a_I = DS_r$, $b_I = SW_l$, $a_{II} = DS_l$, $b_{II} = SW_r$, $c_I = ST_r$, $c_{II} = ST_l$, $d_I = GC_r + \Delta SW$, $d_{II} = GC_l - \Delta SW$, $a_I^{adj} = DS_r^{adj}$, $b_I^{adj} = SW_l^{adj}$, $a_{II}^{adj} = DS_l^{adj}$, $b_{II}^{adj} = SW_r^{adj}$, $c_I^{adj} = ST_r^{adj}$, $c_{II}^{adj} = ST_l^{adj}$, $d_I^{adj} = GC_r^{adj} + \Delta SW^{adj}$, $d_{II}^{adj} = GC_l^{adj} - \Delta SW^{adj}$. The values of the computed Φ-bonacci gait number in (6) (all the gains within it are set equal to 1) are, finally, reported in Table 7.

Table 1. Experimental data concerning the elements (in seconds) of the sequences *I* and *II* in (3) and their adjoint versions I^{adj}, II^{adj} in (4) for the AT patient A ([$DS_x = 0.133$ s, $DS_y = 0.135$ s).

$a_I = DS_r$	$b_I = SW_l$	$c_I = ST_r$	$d_I = GC_r + \Delta SW$
0.268	0.385	0.653	1.038
$a_{II} = DS_l$	$b_{II} = SW_r$	$c_{II} = ST_l$	$d_{II} = GC_l - \Delta SW$
0.259	0.38	0.639	1.019
	SW_l/DS_r	ST_r/SW_l	$(GC_r + \Delta SW)/ST_r$
	1.4366	1.6961	1.5896
	SW_r/DS_l	ST_l/SW_r	$(GC_l - \Delta SW)/ST_l$
	1.4672	1.6816	1.5947
$a_I^{adj} = DS_r^{adj}$	$b_I^{adj} = SW_l^{adj}$	$c_I^{adj} = ST_r^{adj}$	$d_I^{adj} = GC_r^{adj} + \Delta SW^{adj}$
0.268	0.385	0.653	1.038
$a_{II}^{adj} = DS_l^{adj}$	$b_{II}^{adj} = SW_r^{adj}$	$c_{II}^{adj} = ST_l^{adj}$	$d_{II}^{adj} = GC_l^{adj} - \Delta SW^{adj}$
0.224	0.418	0.642	1.06
	SW_l^{adj}/DS_r^{adj}	ST_r^{adj}/SW_l^{adj}	$(GC_r^{adj} + \Delta SW^{adj})/ST_r^{adj}$
	1.4366	1.6961	1.5896
	SW_r^{adj}/DS_l^{adj}	ST_l^{adj}/SW_r^{adj}	$(GC_l^{adj} - \Delta SW^{adj})/ST_l^{adj}$
	1.8661	1.5359	1.6511

Table 2. Experimental data concerning the elements (in seconds) of the sequences *I* and *II* in (3) and their adjoint versions I^{adj}, II^{adj} in (4) for the AT patient F ($DS_x = 1.292$ s, $DS_y = 1.767$ s).

$a_{\text{I}} = DS_r$	$b_{\text{I}} = SW_l$	$c_{\text{I}} = ST_r$	$d_{\text{I}} = GC_r + \Delta SW$
3.0590	0.8370	3.8960	4.7330
$a_{\text{II}} = DS_l$	$b_{\text{II}} = SW_r$	$c_{\text{II}} = ST_l$	$d_{\text{II}} = GC_l - \Delta SW$
2.9510	0.5150	3.4660	3.9810
	SW_l/DS_r	ST_r/SW_l	$(GC_r + \Delta SW)/ST_r$
	0.27362	4.6547	1.2148
	SW_r/DS_l	ST_l/SW_r	$(GC_l - \Delta SW)/ST_l$
	0.17452	6.7301	1.1486
$a_{\text{I}}^{\text{adj}} = DS_r^{\text{adj}}$	$b_{\text{I}}^{\text{adj}} = SW_l^{\text{adj}}$	$c_{\text{I}}^{\text{adj}} = ST_r^{\text{adj}}$	$d_{\text{I}}^{\text{adj}} = GC_r^{\text{adj}} + \Delta SW^{\text{adj}}$
3.0590	0.8370	3.8960	4.7330
$a_{\text{II}}^{\text{adj}} = DS_l^{\text{adj}}$	$b_{\text{II}}^{\text{adj}} = SW_r^{\text{adj}}$	$c_{\text{II}}^{\text{adj}} = ST_l^{\text{adj}}$	$d_{\text{II}}^{\text{adj}} = GC_l^{\text{adj}} - \Delta SW^{\text{adj}}$
2.313	0.488	2.801	3.289
	$SW_l^{\text{adj}}/DS_r^{\text{adj}}$	$ST_r^{\text{adj}}/SW_l^{\text{adj}}$	$(GC_r^{\text{adj}} + \Delta SW^{\text{adj}})/ST_r^{\text{adj}}$
	0.27362	4.6547	1.2148
	$SW_r^{\text{adj}}/DS_l^{\text{adj}}$	$ST_l^{\text{adj}}/SW_r^{\text{adj}}$	$(GC_l^{\text{adj}} - \Delta SW^{\text{adj}})/ST_l^{\text{adj}}$
	0.21098	5.7398	1.1742

Table 3. Experimental data concerning the elements (in seconds) of the sequences *I* and *II* in (3) and their adjoint versions I^{adj}, II^{adj} in (4) for the AT patient G ($DS_x = 0.077$ s, $DS_y = 0.084$ s).

$a_{\text{I}} = DS_r$	$b_{\text{I}} = SW_l$	$c_{\text{I}} = ST_r$	$d_{\text{I}} = GC_r + \Delta SW$
0.161	0.307	0.468	0.775
$a_{\text{II}} = DS_l$	$b_{\text{II}} = SW_r$	$c_{\text{II}} = ST_l$	$d_{\text{II}} = GC_l - \Delta SW$
0.176	0.311	0.487	0.798
	SW_l/DS_r	ST_r/SW_l	$(GC_r + \Delta SW)/ST_r$
	1.9068	1.5244	1.656
	SW_r/DS_l	ST_l/SW_r	$(GC_l - \Delta SW)/ST_l$
	1.7670	1.5659	1.6386
$a_{\text{I}}^{\text{adj}} = DS_r^{\text{adj}}$	$b_{\text{I}}^{\text{adj}} = SW_l^{\text{adj}}$	$c_{\text{I}}^{\text{adj}} = ST_r^{\text{adj}}$	$d_{\text{I}}^{\text{adj}} = GC_r^{\text{adj}} + \Delta SW^{\text{adj}}$
0.161	0.307	0.468	0.775
$a_{\text{II}}^{\text{adj}} = DS_l^{\text{adj}}$	$b_{\text{II}}^{\text{adj}} = SW_r^{\text{adj}}$	$c_{\text{II}}^{\text{adj}} = ST_l^{\text{adj}}$	$d_{\text{II}}^{\text{adj}} = GC_l^{\text{adj}} - \Delta SW^{\text{adj}}$
0.126	0.317	0.443	0.76
	$SW_l^{\text{adj}}/DS_r^{\text{adj}}$	$ST_r^{\text{adj}}/SW_l^{\text{adj}}$	$(GC_r^{\text{adj}} + \Delta SW^{\text{adj}})/ST_r^{\text{adj}}$
	1.9068	1.5244	1.656
	$SW_r^{\text{adj}}/DS_l^{\text{adj}}$	$ST_l^{\text{adj}}/SW_r^{\text{adj}}$	$(GC_l^{\text{adj}} - \Delta SW^{\text{adj}})/ST_l^{\text{adj}}$
	2.5159	1.3975	1.7156

Table 4. Experimental data concerning the elements (in seconds) of the sequences *I* and *II* in (3) and their adjoint versions I^{adj}, II^{adj} in (4) for the healthy subject 1 ($\text{DS}_x = 0.12967$ s, $\text{DS}_y = 0.14$ s).

$a_{\text{I}} = \text{DS}_r$	$b_{\text{I}} = \text{SW}_l$	$c_{\text{I}} = \text{ST}_r$	$d_{\text{I}} = \text{GC}_r + \Delta\text{SW}$
0.2697	0.45133	0.721	1.172
$a_{\text{II}} = \text{DS}_l$	$b_{\text{II}} = \text{SW}_r$	$c_{\text{II}} = \text{ST}_l$	$d_{\text{II}} = \text{GC}_l - \Delta\text{SW}$
0.252	0.421	0.673	1.09
	SW_l/DS_r	ST_r/SW_l	$(\text{GC}_r + \Delta\text{SW})/\text{ST}_r$
	1.6806	1.5992	1.626
	SW_r/DS_l	ST_l/SW_r	$(\text{GC}_l - \Delta\text{SW})/\text{ST}_l$
	1.6985	1.6037	1.6257
$a_{\text{I}}^{\text{adj}} = \text{DS}_r^{\text{adj}}$	$b_{\text{I}}^{\text{adj}} = \text{SW}_l^{\text{adj}}$	$c_{\text{I}}^{\text{adj}} = \text{ST}_r^{\text{adj}}$	$d_{\text{I}}^{\text{adj}} = \text{GC}_r^{\text{adj}} + \Delta\text{SW}^{\text{adj}}$
0.2697	0.45133	0.721	1.172
$a_{\text{II}}^{\text{adj}} = \text{DS}_l^{\text{adj}}$	$b_{\text{II}}^{\text{adj}} = \text{SW}_r^{\text{adj}}$	$c_{\text{II}}^{\text{adj}} = \text{ST}_l^{\text{adj}}$	$d_{\text{II}}^{\text{adj}} = \text{GC}_l^{\text{adj}} - \Delta\text{SW}^{\text{adj}}$
0.256	0.428	0.684	1.112
	$\text{SW}_l^{\text{adj}}/\text{DS}_r^{\text{adj}}$	$\text{ST}_r^{\text{adj}}/\text{SW}_l^{\text{adj}}$	$(\text{GC}_r^{\text{adj}} + \Delta\text{SW}^{\text{adj}})/\text{ST}_r^{\text{adj}}$
	1.6806	1.5992	1.626
	$\text{SW}_r^{\text{adj}}/\text{DS}_l^{\text{adj}}$	$\text{ST}_l^{\text{adj}}/\text{SW}_r^{\text{adj}}$	$(\text{GC}_l^{\text{adj}} - \Delta\text{SW}^{\text{adj}})/\text{ST}_l^{\text{adj}}$
	1.6838	1.6008	1.6257

Table 5. Experimental data concerning the elements (in seconds) of the sequences *I* and *II* in (3) and their adjoint versions I^{adj}, II^{adj} in (4) for the healthy subject 2 ($\text{DS}_x = 0.12633$ s, $\text{DS}_y = 0.123$ s).

$a_{\text{I}} = \text{DS}_r$	$b_{\text{I}} = \text{SW}_l$	$c_{\text{I}} = \text{ST}_r$	$d_{\text{I}} = \text{GC}_r + \Delta\text{SW}$
0.24933	0.39967	0.6490	1.04867
$a_{\text{II}} = \text{DS}_l$	$b_{\text{II}} = \text{SW}_r$	$c_{\text{II}} = \text{ST}_l$	$d_{\text{II}} = \text{GC}_l - \Delta\text{SW}$
0.25933	0.38567	0.64500	1.03067
	SW_l/DS_r	ST_r/SW_l	$(\text{GC}_r + \Delta\text{SW})/\text{ST}_r$
	1.61187	1.62430	1.61623
	SW_r/DS_l	ST_l/SW_r	$(\text{GC}_l - \Delta\text{SW})/\text{ST}_l$
	1.50613	1.67520	1.59860
$a_{\text{I}}^{\text{adj}} = \text{DS}_r^{\text{adj}}$	$b_{\text{I}}^{\text{adj}} = \text{SW}_l^{\text{adj}}$	$c_{\text{I}}^{\text{adj}} = \text{ST}_r^{\text{adj}}$	$d_{\text{I}}^{\text{adj}} = \text{GC}_r^{\text{adj}} + \Delta\text{SW}^{\text{adj}}$
0.24933	0.39967	0.6490	1.04867
$a_{\text{II}}^{\text{adj}} = \text{DS}_l^{\text{adj}}$	$b_{\text{II}}^{\text{adj}} = \text{SW}_r^{\text{adj}}$	$c_{\text{II}}^{\text{adj}} = \text{ST}_l^{\text{adj}}$	$d_{\text{II}}^{\text{adj}} = \text{GC}_l^{\text{adj}} - \Delta\text{SW}^{\text{adj}}$
0.24867	0.39367	0.64233	1.0360
	$\text{SW}_l^{\text{adj}}/\text{DS}_r^{\text{adj}}$	$\text{ST}_r^{\text{adj}}/\text{SW}_l^{\text{adj}}$	$(\text{GC}_r^{\text{adj}} + \Delta\text{SW}^{\text{adj}})/\text{ST}_r^{\text{adj}}$
	1.61187	1.62430	1.61623
	$\text{SW}_r^{\text{adj}}/\text{DS}_l^{\text{adj}}$	$\text{ST}_l^{\text{adj}}/\text{SW}_r^{\text{adj}}$	$(\text{GC}_l^{\text{adj}} - \Delta\text{SW}^{\text{adj}})/\text{ST}_l^{\text{adj}}$
	1.59027	1.63530	1.61250

Table 6. Experimental data concerning the elements (in seconds) of the sequences *I* and *II* in (3) and their adjoint versions I^{adj}, II^{adj} in (4) for the healthy subject 3 ($\text{DS}_x = 0.11733$ s, $\text{DS}_y = 0.12133$ s).

$a_{\text{I}} = \text{DS}_r$	$b_{\text{I}} = \text{SW}_l$	$c_{\text{I}} = \text{ST}_r$	$d_{\text{I}} = \text{GC}_r + \Delta\text{SW}$
0.23867	0.3830	0.62167	1.00467
$a_{\text{II}} = \text{DS}_l$	$b_{\text{II}} = \text{SW}_r$	$c_{\text{II}} = \text{ST}_l$	$d_{\text{II}} = \text{GC}_l - \Delta\text{SW}$
0.24267	0.3960	0.63867	1.03467
	SW_l/DS_r	ST_r/SW_l	$(\text{GC}_r + \Delta\text{SW})/\text{ST}_r$
	1.60573	1.62333	1.61607
	SW_r/DS_l	ST_l/SW_r	$(\text{GC}_l - \Delta\text{SW})/\text{ST}_l$
	1.6320	1.61370	1.61987
$a_{\text{I}}^{\text{adj}} = \text{DS}_r^{\text{adj}}$	$b_{\text{I}}^{\text{adj}} = \text{SW}_l^{\text{adj}}$	$c_{\text{I}}^{\text{adj}} = \text{ST}_r^{\text{adj}}$	$d_{\text{I}}^{\text{adj}} = \text{GC}_r^{\text{adj}} + \Delta\text{SW}^{\text{adj}}$
0.23867	0.3830	0.62167	1.00467
$a_{\text{II}}^{\text{adj}} = \text{DS}_l^{\text{adj}}$	$b_{\text{II}}^{\text{adj}} = \text{SW}_r^{\text{adj}}$	$c_{\text{II}}^{\text{adj}} = \text{ST}_l^{\text{adj}}$	$d_{\text{II}}^{\text{adj}} = \text{GC}_l^{\text{adj}} - \Delta\text{SW}^{\text{adj}}$
0.23367	0.4090	0.64267	1.05167
	$\text{SW}_l^{\text{adj}}/\text{DS}_r^{\text{adj}}$	$\text{ST}_r^{\text{adj}}/\text{SW}_l^{\text{adj}}$	$(\text{GC}_r^{\text{adj}} + \Delta\text{SW}^{\text{adj}})/\text{ST}_r^{\text{adj}}$
	1.60573	1.62333	1.61607
	$\text{SW}_r^{\text{adj}}/\text{DS}_l^{\text{adj}}$	$\text{ST}_l^{\text{adj}}/\text{SW}_r^{\text{adj}}$	$(\text{GC}_l^{\text{adj}} - \Delta\text{SW}^{\text{adj}})/\text{ST}_l^{\text{adj}}$
	1.78253	1.57800	1.63620

Table 7. The values of the computed Φ-bonacci gait number in (6) (all the gains within it are set equal to 1).

AT patient A.	$\mathcal{Y}_\Phi = 0.37838$
AT patient F.	$\mathcal{Y}_\Phi = 6.0926$
AT patient G.	$\mathcal{Y}_\Phi = 0.72389$
Healthy subject 1.	$\mathcal{Y}_\Phi = 0.22046$
Healthy subject 2.	$\mathcal{Y}_\Phi = 0.17933$
Healthy subject 3.	$\mathcal{Y}_\Phi = 0.1811$

4. Discussion

Due to the lack of decisive solutions, AT remains a disabling progressive chronic condition, especially in its classic form, requiring huge personal and family commitment in terms of time, money, and lifelong rehabilitative programs. Hopefully, neurorehabilitation has developed ,in recent years, new opportunities to minimize and/or compensate for functional alterations and/or neurological disability; this is achieved, rather, by addressing different types of therapy to specific clinical disorders and patients' age. However, thanks to the growing body of knowledge, traditional rehabilitative approaches are now more often flanked by fascinating experimental investigations leading to the more independent management of the disease from the patient's point of view, while alsoallowing more frequent and long-lasting patient training. In particular, instrumental gait analysis allows for objectively assessing important parameters related to the locomotor ability of subjects with neurological diseases, although in many neurodegenerative syndromes these analyses have not yet been investigated.

Now, according to the previous section and in particular to Table 7, the Φ-bonacci gait number turns out to be larger for the AT patients than the healthy subjects. Furthermore, among the three healthy subjects, the values of this index consistently range from 0.179 to 0.221. The largest values of this index—observed in AT patients—reflect the effects of their

pathology. Among them, patient A—with the mildest AT phenotype—exhibits the smallest number, despite it being approximately twice as large as the healthy subjects'. Patient G—with an intermediate AT phenotype—exhibits an index that is, in turn, approximately twice as large as patient A.'s. Lastly, a very high value of this index is computed for patient F, who has the most severe AT phenotype. It is worth noticing that the mere analysis of the double support phase durations does not allow us to highlight all these quantitative considerations. In fact, as shown in the related tables, the durations of the double support phases for patient A are similar to those corresponding to the healthy subjects, whereas the same durations for patient G are even lower than those corresponding to healthy subjects. Only for patient F, are these durations are meaningfully large. These results, which comply with the relevant qualitative evaluations provided by the clinicians, support the idea that the Φ-bonacci gait number can be successfully used in a rare disease such as AT. In more detail, despite a study on a wider sample being needed, these data are sufficient to find statistically significant differences between the patients and the healthy controls ($p = 0.05$, Mann–Whitney one tailed U test). The data for the most severe patient (F) exhibit the highest value of the Φ-bonacci gait number, confirming not only the accuracy of this index in differentiating the patients from the healthy subjects, but also to objectively quantify the deficit among the patients.

Therefore, the use of objective measures of motor abilities in AT patients, such as the ones described in this paper, might facilitate the standardization of rehabilitative treatments and the evaluation of outcomes. These can help, first, in identifying predictors of the progression of motor and movement dysfunctions, and, next, facilitate patient selection and stratification in clinical trials, potentially enabling studies with direct clinical outcomes, which can be hindered, mostly, by inter- and intrasubject variability regarding severity and progression of the disease. Concurrently, in home evaluation through objective measures of motor abilities might minimize difficulties in accessing specialized clinical care for disabled AT people and those living in underserved areas, highlighting the need for the latest strategies involving telemedicine.

5. Further Applications

This section aims at showing that the wearable motion capture system adopted in this paper also allows for evaluating motor imagery (MI), which is an important resource in neurorehabilitation. Defined as a multiprofessional physician led approach to healthcare, it aims at reducing disability and improving functions affected by damaged nervous systems [37]. MI is a cognitive process in which the representation of a given motor movement is executed in working memory without any motor output [38]. This process is embedded in a mental imagery construct—a multimodal cognitive simulation process that enables us to represent perceptual information in our minds in the absence of actual sensory input [39]—and refers specifically to the mental simulation of body movements. The use of MI turns out to be relevant in movement disorders. Indeed, MI has been explored in clinical groups, e.g., patients with movement disorders and specific neurological diseases [40–42].

In respect to this, the three AT patients were required to start an additional experiment (see [43]) by standing over a line marked on the floor. In front of them, another line was taped on the ground at a distance (unknown to the subjects) of 9 m (4.5 m for F). They were first asked to stand still and imagine moving towards the visualized target (referred to as MIs). Then, subjects were requested to imagine the same task by mimicking the physical movements of walking (referred to as MIw) (F did not carried out this activity). To verify the ability to perform such imaginary tasks, the time of MI was calculated by a chronometer (referred to as T) and compared to the time spent to reach the target. The results are reported below.

- A (9 m): T = 6.8 s — MIs = 6.23 s — MIw = 5.4 s
- F (4.5 m): T = 35.7 s — MIs = 23.94 s —MIw = n.a.
- G (9 m): T = 7.8 s — MIs = 4.96 s — MIw = 8.18 s

The MI tests provide interesting information about the implicit awareness of pathology severity in patients. Patient A shows a good temporal equivalence between the real execution of the task and the two motor imagery tasks. This equivalence is preserved for the dynamic MI of patient G, whereas the imagined time during the static task is shorter, for patients F and G, than the one corresponding to their real walking, according to the idea that patients may often underestimate their deficits [43].

6. Strengths and Limits

The main advantage of the Φ-*bonacci gait number* (6) is to consider, in a comprehensive manner, the recursivity, symmetry, and harmony of walking in terms of gait phases. The strength of this paper lies in it being the first experimental validation of such an index (recall that, in [25], a simplified version of the index was used, owing to partial data availability) of a class of patients with a rare disease, such as AT. The current core ingredient of an innovative approach to neurorehabilitation is, in fact, the possibility to objectively compute crucial parameters related to the locomotor ability of subjects with neurological diseases. Nevertheless, the limits of the present study mainly lie in the small size of the samples enrolled, though AT is a rare genetic disorder. Furthermore, no responsiveness to changes obtained with rehabilitation has been tested at the present stage.

7. Conclusions

Easy to use wearable motion capture systems can be used to evaluate motion abilities in AT through the objective recursivity and harmonicity and symmetry outcome measures of [25]. The level of the distortions of the harmonic/symmetric temporal proportions is thus quantified through the characterization of the related alterations. The values of the involved indices are shown to comply with the qualitative evaluations provided by the clinicians.

Further attention will be devoted to incorporating these promising results into the framework of gaming technologies (e.g., virtual reality and exergames). Such technologies have been increasingly used in recent years, as they improve the effectiveness of neurorehabilitation, in particular for children with neurological disorders, making it more appealing and enjoyable [44] and usable in family settings [44]. Indeed, there is increasing experimental evidence that virtual technologies may also promote artistic interventions that might be beneficial, particularly to certain populations of patients (i.e., children with rare diseases) for remote rehabilitative purposes [45].

Author Contributions: Conceptualization: C.M.V., M.I., A.E.G., M.R., A.P.; methodology: C.M.V., M.I.; software and resources: M.E.A., G.S.; formal analysis: M.E.A., C.M.V., M.I.; validation, investigation: L.C., M.R., A.P.; writing—original draft: M.E.A., C.M.V., G.S., M.I., A.E.G., L.C., M.R., A.P.; writing—review and editing: C.M.V., M.I., G.S., A.E.G., M.R., A.P. All authors have read and agreed to the published version of the manuscript.

References

1. Chessa, L.; Polizzi, A.; Ruggieri, M. Ataxia-Telangiectasia. In *Neurocutaneous Diseases. Phakomatoses and Hamartoneoplastic Syndromes*; Ruggieri, M., Pascual-Castroviejo, I., Di Rocco, C., Eds.; Springer: New York, NY, USA; 2018; pp. 731–758.
2. Chessa, L.; Ruggieri, M.; Polizzi, A. Progress and prospects for treating Ataxia Telangiectasia. *Expert Opin. Orphan Drugs* **2019**, *7*, 233–251. [CrossRef]
3. Levy, A.; Lang, A.E. Ataxia Telangiectasia: A review of movement disorders, clinical features, and genotype correlations. *Mov. Disord.* **2018**, *33*, 1238–1247. [CrossRef] [PubMed]
4. Liu, H.; Allen, J.; Zheng, D.; Chen, F. The recent development of respiratory rate measurement technologies. *Physiol. Meas.* **2019**, *40*, 07TR01. [CrossRef] [PubMed]
5. Saeed, U.; Shah, S.Y.; Shah, S.A.; Liu, H.; Alotaibi, A.A.; Althobaiti, T.; Ramzan, N.; Jan, S.U.; Ahmad, J.; Abbasi, Q.H. Multiple participants' discrete activity recognition in a well-controlled environment using universal software radio peripheral wireless sensing. *Sensors* **2022**, *22*, 809. [CrossRef] [PubMed]
6. Ricci, M.; di Lazzaro, G.; Pisani, A.; Mercuri, N.B.; Giannini, F.; Saggio, G. Assessment of motor impairments in early untreated parkinson's disease patients: the wearable electronics impact. *IEEE J. Biomed. Health Inform.* **2019**, *24*, 120–130. [CrossRef]
7. Saggio, G.; Quitadamo, L.R.; Albero, L. Development and evaluation of a novel low-cost sensor-based knee flexion angle measurement system. *Knee* **2014**, *21*, 896–901. [CrossRef]
8. Prasanth, H.; Caban, M.; Keller, U.; Courtine, G.; Ijspeert, A.; Vallery, H.; von Zitzewitz, J. Wearable sensor-based real-time gait detection: A systematic review. *Sensors* **2021**, *21*, 2727. [CrossRef]
9. Picerno, P.; Iosa, M.; D'Souza, C.; Benedetti, M.G.; Paolucci, S.; Morone, G. Wearable inertial sensors for human movement analysis: A five-year update. *Expert Rev. Med. Devices* **2021**, *18* (Suppl. 1), 79–94. [CrossRef]
10. Vilas-Boas, M.d.C.; Cunha, J.P.S. Movement quantification in neurological diseases: Methods and applications. *IEEE Rev. Biomed. Eng.* **2016**, *9*, 15–31. [CrossRef]
11. Ren, P.; Zhao, W.; Zhao, Z.; Bringas-Vega, M.L.; Valdes-Sosa, P.A.; Kendrick, K.M. Analysis of gait rhythm fluctuations for neurodegenerative diseases by phase synchronization and conditional entropy. *IEEE Trans. Neural Syst. Rehabil. Eng.* **2016**, *24*, 291–299. [CrossRef]
12. Salarian, A.; Russmann, H.; Vingerhoets, F.J.G.; Dehollain, C.; Blanc, Y.; Burkhard, P.R.; Aminian, K. Gait assessment in Parkinson's disease: Toward an ambulatory system for long term monitoring. *IEEE Trans. Biomed. Eng.* **2004**, *51*, 1434–1443. [CrossRef]
13. Serrao, M.; Chini, G.; Iosa, M.; Casali, C.; Morone, G.; Conte, C.; Bini, F.; Marinozzi, F.; Coppola, G.; Pierelli, F.; et al. Harmony as a convergence attractor that minimizes the energy expenditure and variability in physiological gait and the loss of harmony in cerebellar ataxia. *Clin. Biomech.* **2017**, *48*, 15–23. [CrossRef]
14. Ricci, M.; Terribili, M.; Giannini, F.; Errico, V.; Pallotti, A.; Galasso, C.; Tomasello, L.; Sias, S.; Saggio, G. Wearable-based electronics to objectively support diagnosis of motor impairments in school-aged children. *J. Biomech.* **2019**, *83*, 243–252. [CrossRef]
15. Wang, J.-S.; Lin, C.-W.; Yang, Y.-T.C.; Ho, Y.-J. Walking pattern classification and walking distance estimation algorithms using gait phase information. *IEEE Trans. Biomed. Eng.* **2012**, *59*, 2884–2892. [CrossRef]
16. Dugan, S.A.; Bat, K.P. Biomechanics and analysis of running gait. *Phys. Med. Rehabil. Clin. North Am.* **2005**, *16*, 603–621. [CrossRef]
17. Greene, B.R.; McGrath, D.; O'Neill, R.; O'Donovan, K.J.; Burns, A.; Caulfield, B. An adaptive gyroscope-based algorithm for temporal gait analysis. *Med. Biol. Eng. Comput.* **2010**, *48*, 1251–1260. [CrossRef]
18. Saggio, G.; Sbernini, L. New scenarios in human trunk posture measurements for clinical applications. In Proceedings of the 2011 IEEE International Symposium on Medical Measurements and Applications, Bari, Italy, 30–31 May 2011 ; pp. 13–17.
19. Iosa, M.; Fusco, A.; Marchetti, F.; Morone, G.; Caltagirone, C.; Paolucci, S.; Peppe, A. The golden ratio of gait harmony: Repetitive proportions of repetitive gait phases. *BioMed Res. Int.* **2013**, *2013*, 1–7. [CrossRef]
20. Cavagna, G.A.; Margaria, R. Mechanics of walking. *J. Appl. Physiol.* **1966**, *21*, 271–278. [CrossRef]
21. Marino, R.; Verrelli, C.M.; Gnucci, M. Synchronicity rectangle for temporal gait analysis: Application to Parkinson's Disease. *Biomed. Signal Process. Control* **2020**, *62*, 102156. [CrossRef]
22. Iosa, M.; Morone, G.; Fusco, A.; Marchetti, F.; Caltagirone, C.; Paolucci, S.; Peppe, A. Loss of fractal gait harmony in Parkinson's Disease. *Clin. Neurophysiol.* **2016**, *127*, 1540–1546. [CrossRef]
23. Iosa, M.; Bini, F.; Marinozzi, F.; Fusco, A.; Morone, G.; Koch, G.; Cinnera, A.M.; Bonní, S.; Paolucci, S. Stability and harmony of gait in patients with subacute stroke. *J. Med. Biol. Eng.* **2016**, *36*, 635–643. [CrossRef]
24. Pasciuto, I.; Bergamini, E.; Iosa, M.; Vannozzi, G.; Cappozzo, A. Overcoming the limitations of the Harmonic Ratio for the reliable assessment of gait symmetry. *J. Biomech.* **2017**, *53*, 84–89. [CrossRef]
25. Verrelli, C.M.; Iosa, M.; Roselli, P.; Pisani, A.; Giannini, F.; Saggio, G. Generalized finite-length Fibonacci sequences in healthy and pathological human walking: Comprehensively assessing recursivity, asymmetry, consistency, self-Similarity, and variability of gaits. *Front. Hum. Neurosci.* **2021**, *15*, 649533. [CrossRef]
26. Hausdorff, J.M.; Peng, C.-K.; Ladin, Z.; Wei, J.Y.; Goldberger, A.L. Is walking a random walk? Evidence for long-range correlations in the stride interval of human gait. *J. Appl. Physiol.* **1995**, *78*, 349–358. [CrossRef]
27. Hausdorff, J.M.; Schaafsma, J.D.; Balash, Y.; Bartels, A.L.; Gurevich, T.; Giladi, N. Impaired regulation of stride variability in Parkinson's disease subjects with freezing of gait. *Exp. Brain Res.* **2003**, *149*, 187–194. [CrossRef] [PubMed]
28. Verrelli, C.M.; Romagnoli, C.; Jackson, R.R.; Ferretti, I.; Annino, G.; Bonaiuto, V. Front crawl stroke in swimming: Ratios of phase durations and self-similarity. *J. Biomech.* **2021**, *118*, 110267. [CrossRef]

29. Verrelli, C.M.; Romagnoli, C.; Jackson, R.R.; Ferretti, I.; Annino, G.; Bonaiuto, V. Phi-bonacci Butterfly Stroke Numbers to Assess Self-Similarity in Elite Swimmers. *Mathematics* **2021**, *9*, 1545. [CrossRef]

30. Horadam, A.F. A generalized Fibonacci sequence. *Am. Math. Mon.* **1961**, *68*, 455-459. [CrossRef]

31. Kavanagh, J.J.; Morrison, S.; James, D.A.; Barrett, R. Reliability of segmental accelerations measured using a new wireless gait analysis system. *J. Biomech.* **2006**, *39*, 2863–2872. [CrossRef] [PubMed]

32. Potdevin, F.J.; Femery, V.G.; Decatoire, A.; Bosquet, L.; Coello, Y.; Moretto, P. Using effect size to quantify plantar pressure asymmetry of gait of nondisabled adults and patients with hemiparesis. *J. Rehabil. Res. Dev.* **2007**, *44*, 347–354. [CrossRef] [PubMed]

33. Kirtley, C. *Clinical Gait Analysis—Theory and Practice*; Elsevier Health Sciences, Churchill Livingstone: Edinburgh, Scotland, 2006.

34. Błażkiewicz, M.; Wiszomirska, I.; Wit, A. Comparison of four methods of calculating the symmetry of spatial-temporal parameters of gait. *Acta Bioeng. Biomech.* **2014**, *16*, 29–35.

35. Saggio, G.; Tombolini, F.; Ruggiero, A. Technology-based complex motor tasks assessment: A 6-DOF inertial-based system versus a gold-standard optoelectronic-based one. *IEEE Sens. J.* **2020**, *21*, 1616–1624. [CrossRef]

36. Hughes, S.; Liu, H.; Zheng, D. Influences of sensor placement site and subject posture on measurement of respiratory frequency using triaxial accelerometers. *Front. Physiol.* **2020**, *11*, 823. [CrossRef]

37. Platz, T.; Sandrini, G. Specialty grand challenge for NeuroRehabilitation research. *Front Neurol.* **2020**, *11*, 349. [CrossRef]

38. Decety, J. Neural representations for action. *Rev Neurosci.* **1996**, *7*, 285–297. [CrossRef]

39. Munzert, J.; Lorey, J.; Zentgraf, J. Cognitive motor processes: the role of motor imagery in the study of motor representations. *Brain Res. Rev.* **2009**, *60*, 306–326. [CrossRef]

40. de Bartolo, D.; Belluscio, V.; Vannozzi, G.; Morone, G.; Antonucci, G.; Giordani, G.; Santucci, S.; Resta, F.; Marinozzi, F.; Bini, F.; et al. Sensorized assessment of dynamic locomotor imagery in people with stroke and healthy subjects. *Sensors* **2020**, *20*, 4545. [CrossRef]

41. Cuomo, G.; Maglianella, V.; Ghooshchy, S.G.; Zoccolotti, P.; Martelli, M.; Paolucci, S.; Morone, G.; Iosa, M. Motor imagery and gait control in Parkinson's disease: Techniques and new perspectives in neurorehabilitation. *Expert Rev. Neurother.* **2021**, *1*, 43–51. [CrossRef]

42. Huang, H.C.; Chen, C.M.; Lu, M.K.; Liu, B.L.; Li, C.I.; Chen, J.C.; Wang, G.J.; Lin, H.C.; Duann, J.R.; Tsai, C.H. Gait-related brain activation during motor imagery of complex and simple ambulation in Parkinson's Disease with freezing of gait. *Front. Aging Neurosci.* **2021**, *13*, 731332. [CrossRef]

43. Fusco, A.; Gallotta, M.C.; Iosa, M.; Morone, G.; Iasevoli, L.; Trifoglio, D.; Saraceni, V.M.; Paolucci, S.; Baldari, C.; Guidetti, L. The dynamic motor imagery of locomotion is task-dependent in patients with stroke. *Restor. Neurol. Neurosci.* **2016**, *34*, 247–256. PMID: 26889966. [CrossRef]

44. Iosa, M.; Verrelli, C.M.; Gentile, A.E.; Ruggieri, M.; Polizzi, A. Gaming technology for pediatric neurorehabilitation: A systematic review. *Front. Pediatr.* **2022**, *10*, 775356. [CrossRef] [PubMed]

45. Polizzi, A.; Gentile, A.E.; Taruscio, D. Competing to raise awareness of rare diseases. *Lancet Neurol.* **2019**, *18*, 721-722. [CrossRef]